Time-Modulated Antenna Array with Dual-Circular Polarization

Grzegorz Bogdan, *Member, IEEE,* Paweł Bajurko, *Member, IEEE,* and Yevhen Yashchyshyn, *Senior Member, IEEE*

***Abstract*—This letter presents a time-modulated antenna array (TMAA) with a dual-circular (left-hand and right-hand) polarization. The TMAA is composed of a single-pole four-throw (SP4T) radio-frequency (RF) switch and four linearly polarized elements arranged accordingly to the sequential rotation technique. A periodic switching of the elements leads to generation of sideband components in the frequency domain. The right-hand circular polarization (RHCP) and the left-hand circular polarization (LHCP) are synthesized over the first negative sideband frequency and the first positive sideband frequency, respectively, in wide frequency band. The TMAA used in the receiving mode provides conversion of the polarization-diversity into the frequency-diversity, therefore enables simultaneous reception and automatic separation of two electromagnetic waves which have the same frequency, however, mutually orthogonal senses of polarization.**

***Index Terms*—antenna arrays, circular polarization, dual-polarized antennas, time-modulated antenna arrays**

I. Introduction

POLARIZATION is one of the key parameters in antenna design. It specifies the shape, orientation, and sense of the ellipse that the extremity of the field vector describes as a function of time [1]. In order to obtain a circular polarization the magnitudes of the two orthogonal components of the electric-field have to be the same and the phase difference between them have to be odd multiples of 90° [2]. It can be achieved with a sequential rotation technique [3], [4], which uses an array of linearly-polarized elements which are sequentially rotated, normally by 90° between adjacent elements. In order to obtain the required mutual phase-relation between each element's radiated field, the rotation is complemented with a phase-shift in the feeding network. It is typically realized with a sequential-phase feed [5]–[7], a hybrid coupler [8], or the Buttler matrix [9]; however, the performance of these conventional methods depends on the frequency.

A time-modulated antenna array (TMAA) is based on a periodic on-off switching of its elements [10]. The periodic modulation of a TMAA generates sidebands in the form of spectral components at frequencies shifted from the carrier frequency at multiples of the time-modulation rate [11]. The presence of sidebands used to be considered as undesirable, therefore a significant research effort had been made toward optimization of linear [12], planar [13], circular [14], conformal [15], and reconfigurable [16] TMAAs.

The authors are with the Warsaw University of Technology, Warsaw 00-665, Poland (e-mail: g.bogdan@ire.pw.edu.pl; p.bajurko@ire.pw.edu.pl; y.yashchyshyn@ire.pw.edu.pl).

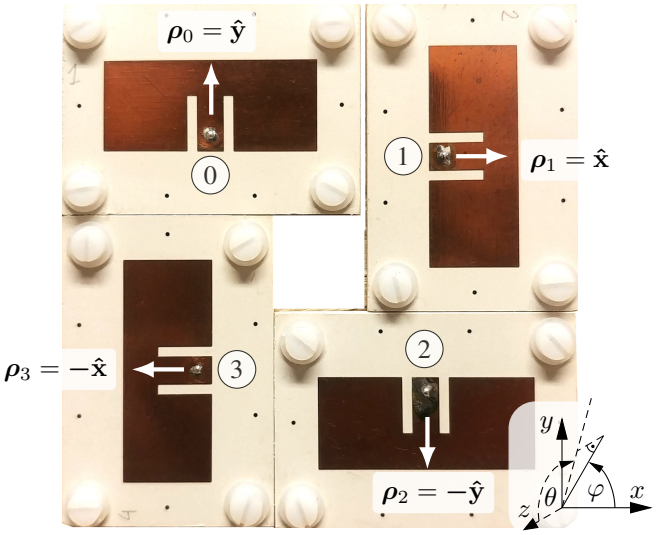

Fig. 1. Design of dual-circular polarized TMAA. The elements are enumerated with integer numbers in a clockwise order and annotated with arrows which indicate direction of the polarization vector.

The proposed TMAA is composed of four sequentially rotated elements and a single-pole four-throw (SP4T) radio-frequency (RF) switch, which is utilized instead of a conventional sequential-phase feed. Such a TMAA is capable of generating orthogonal components of the electric field vector, hence it can be used to obtain either a linear polarization (when the periodic switching is realized between two oppositely oriented elements) or a circular polarization. In this paper the focus is on the circular polarization due to its advantageous property in comparison to conventional mechanisms of the sequential-phase feed, i.e. performance of the TMAA in terms of the axial ratio (AR) is independent of the frequency. The TMAA is dual-circular polarized, because it demonstrates the right-hand circular polarization (RHCP) and the left-hand circular polarization (LHCP) over the first negative sideband frequency and the first positive sideband frequency, respectively. Therefore, it can be used for simultaneous reception (or transmission) of two orthogonal circularly-polarized waves.

II. TMAA with Dual-Circular Polarization

A. Design of TMAA

The TMAA consists of $N = 4$ linearly polarized elements arranged in accordance to the sequential rotation technique.

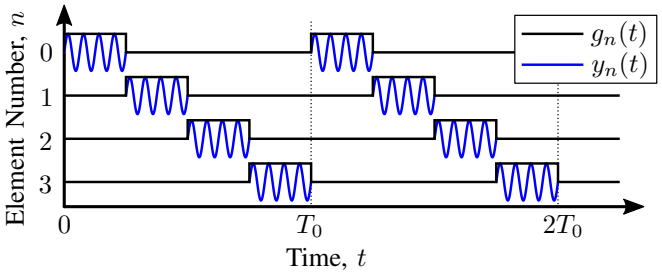

Fig. 2. Illustration of signals at throws of the SP4T switch.

An exemplary design composed of E-shaped patch antennas for 5.0–5.7 GHz band is presented in Fig. 1. Polarization vectors of the elements $\boldsymbol{\rho}_0 = \hat{\mathbf{y}}$ and $\boldsymbol{\rho}_1 = \hat{\mathbf{x}}$ are opposite to $\boldsymbol{\rho}_2 = -\hat{\mathbf{y}}$ and $\boldsymbol{\rho}_3 = -\hat{\mathbf{x}}$, respectively. The HMC345LP3 SP4T RF switch is used to periodically connect/disconnect array elements to/from the feeding line. The construction of the switch imposes that one of the throws is always connected to the feeding line, while other throws are internally terminated to 50 Ω. It prevents power losses during the off-state, hence safeguards the efficiency [17], [18].

B. Mathematical Formulation

Elements of the proposed TMAA can be time-modulated in a periodic, uniform and sequential manner, i.e. consecutive throws of the SP4T RF switch can be enabled in order (from 0 to 3) for duration of $T_0/4$, where T_0 denotes the period. Hence, the switching of n-th element can be represented by means of an unipolar function:

$$g_n(t) = \begin{cases} 1, \text{ if } aT_0 + n\frac{T_0}{4} \leq t < aT_0 + (n+1)\frac{T_0}{4} \\ 0, \text{ otherwise} \end{cases} \tag{1}$$

for any $a \in \mathbb{Z}$ and $n = 0, \ldots, N-1$. If the pole of the SP4T RF switch is fed by an RF signal $s(t) = e^{j2\pi f_c t}$, where f_c is the carrier frequency, then an output signal at the n-th throw of the switch is:

$$y_n(t) = s(t) \cdot g_n(t). \tag{2}$$

Waveforms of $g_n(t)$ and $y(t)$ are illustrated in Fig. 2. Signals $g_n(t)$ and $s_n(t)$ are Fourier transformable:

$$s(t) \overset{\mathfrak{F}}{\Longleftrightarrow} \delta(f - f_c) \tag{3}$$

$$g_n(t) \overset{\mathfrak{F}}{\Longleftrightarrow} G_n(f) = \sum_{k=-\infty}^{\infty} G_n^{(k)} \cdot \delta(f - kf_0), \tag{4}$$

where $k \in \mathbb{Z}$, $f_0 = 1/T_0$ is the switching rate, $G_n^{(k)}$ denotes complex Fourier coefficients, and δ is the Dirac delta function. The Fourier transform of (2) can be expressed as a convolution of (3) and (4):

$$\begin{aligned} y_n(t) \overset{\mathfrak{F}}{\Longleftrightarrow} Y_n(f) &= \delta(f - f_c) * G_n(f) = \\ &\delta(f - f_c) * \sum_{k=-\infty}^{\infty} G_n^{(k)} \cdot \delta(f - kf_0) = \\ &\sum_{k=-\infty}^{\infty} G_n^{(k)} \cdot \delta(f - f_c - kf_0) \end{aligned} \tag{5}$$

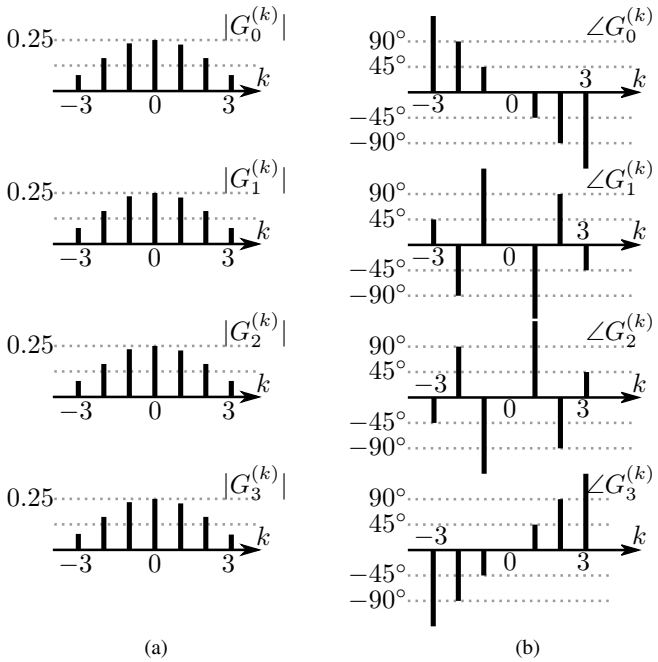

Fig. 3. Discrete spectrum of modulated signals (a) Magnitude spectra (b) Phase spectra.

TABLE I
PHASE SPECTRA OF MODULATED SIGNALS

n	$\angle G_n^{(-2)}$	$\angle G_n^{(-1)}$	$\angle G_n^{(0)}$	$\angle G_n^{(1)}$	$\angle G_n^{(2)}$
0	90°	45°	0°	−45°	−90°
1	−90°	135°	0°	−135°	90°
2	90°	−135°	0°	135°	−90°
3	−90°	−45°	0°	45°	90°

A non-zero values of $Y_n(f)$ are obtained only at discrete frequencies $f_c + kf_0$. Thus, a discrete spectrum $Y_n^{(k)}$ can be expressed as follows:

$$Y_n^{(k)} = Y_n(f_c + kf_0) = G_n^{(k)} \tag{6}$$

According to (6) the spectrum of a time-modulated signal is composed of the center frequency component ($k = 0$) and an infinite number of discrete sideband components ($k \in \mathbb{Z} \ \wedge \ k \neq 0$).

Magnitude spectra $|G_n^{(k)}|$ and phase spectra $\angle G_n^{(k)}$ of $y_n(t)$ are presented in Fig. 3a and Fig. 3b, respectively. Magnitude spectra are identical, therefore the notation can be simplified by omitting the index n: $|G_n^{(k)}| = |G^{(k)}| \ \forall \ n = 0, \ldots, N-1$. The phase spectra are different. Their values for $k = \{-2, -1, 0, 1, 2\}$ are gathered in Tab. I. Almost 86% of the total signal energy is carrier by spectral components with orders $k = \{-2, -1, 0, 1, 2\}$.

C. Polarization Analysis

The electric field vector of the wave radiated in the broadside direction ($\theta = 0°$) is proportional to the superposition of the waves radiated by all elements:

$$\boldsymbol{E}_B \propto \sum_{k=-\infty}^{+\infty} \sum_{n=0}^{N-1} G_n^{(k)} \boldsymbol{\rho}_n \tag{7}$$

The electric field vector can be analyzed for each spectral component separately.

1) The center frequency ($k = 0$): According to (8) electric field vectors radiated by the elements are oppositely oriented, therefore a broadside null is produced.

$$\boldsymbol{E}_B^{(0)} \propto |G_0^{(0)}|e^{j0^\circ}\hat{\mathbf{y}} + |G_1^{(0)}|e^{j0^\circ}\hat{\mathbf{x}} + - |G_2^{(0)}|e^{j0^\circ}\hat{\mathbf{y}} - |G_3^{(0)}|e^{j0^\circ}\hat{\mathbf{x}} = 0 \quad (8)$$

2) The first negative sideband component ($k = -1$): According to (9) magnitudes of the electric field for both the horizontal vector (along the x-axis) and the vertical vector (along the y-axis) are the same and the phase-difference between them equals $+90^\circ$, therefore the RHCP is obtained.

$$\begin{aligned}\boldsymbol{E}_B^{(-1)} &\propto |G_0^{(-1)}|e^{j45^\circ}\hat{\mathbf{y}} + |G_1^{(-1)}|e^{j135^\circ}\hat{\mathbf{x}} + \\ &- |G_2^{(-1)}|e^{-j135^\circ}\hat{\mathbf{y}} - |G_3^{(-1)}|e^{-j45^\circ}\hat{\mathbf{x}} = \\ &|G^{(-1)}|\left(e^{j45^\circ}\hat{\mathbf{y}} + e^{j135^\circ}\hat{\mathbf{x}} + e^{j45^\circ}\hat{\mathbf{y}} + e^{j135^\circ}\hat{\mathbf{x}}\right) = \\ &2|G^{(-1)}|\left(e^{j135^\circ}\hat{\mathbf{x}} + e^{j45^\circ}\hat{\mathbf{y}}\right) \quad (9)\end{aligned}$$

3) The first positive sideband component ($k = 1$): According to (10) magnitudes of the electric field for both the horizontal vector and the vertical vector are the same and the phase-difference between them equals -90°, therefore the LHCP is obtained.

$$\begin{aligned}\boldsymbol{E}_B^{(1)} &\propto |G_0^{(1)}|e^{-j45^\circ}\hat{\mathbf{y}} + |G_1^{(1)}|e^{-j135^\circ}\hat{\mathbf{x}} + \\ &- |G_2^{(1)}|e^{j135^\circ}\hat{\mathbf{y}} - |G_3^{(1)}|e^{j45^\circ}\hat{\mathbf{x}} = \\ &|G^{(1)}|\left(e^{-j45^\circ}\hat{\mathbf{y}} + e^{-j135^\circ}\hat{\mathbf{x}} + e^{-j45^\circ}\hat{\mathbf{y}} + e^{-j135^\circ}\hat{\mathbf{x}}\right) = \\ &2|G^{(1)}|\left(e^{-j135^\circ}\hat{\mathbf{x}} + e^{-j45^\circ}\hat{\mathbf{y}}\right) \quad (10)\end{aligned}$$

4) The second negative sideband component ($k = -2$): According to (11) the second negative sideband component is suppressed in the broadside direction.

$$\boldsymbol{E}_B^{(-2)} \propto |G_0^{(-2)}|e^{j90^\circ}\hat{\mathbf{y}} + |G_1^{(-2)}|e^{-j90^\circ}\hat{\mathbf{x}} + - |G_2^{(-2)}|e^{j90^\circ}\hat{\mathbf{y}} - |G_3^{(-2)}|e^{-j90^\circ}\hat{\mathbf{x}} = 0 \quad (11)$$

5) The second positive sideband component ($k = 2$): According to (12) the second positive sideband component is suppressed in the broadside direction.

$$\boldsymbol{E}_B^{(2)} \propto |G_0^{(2)}|e^{-j90^\circ}\hat{\mathbf{y}} + |G_1^{(2)}|e^{j90^\circ}\hat{\mathbf{x}} + - |G_2^{(2)}|e^{-j90^\circ}\hat{\mathbf{y}} - |G_3^{(2)}|e^{j90^\circ}\hat{\mathbf{x}} = 0 \quad (12)$$

The spectral analysis of the TMAA output signal leads to the following observations:

1) the RHCP is synthesized over $k = -1$,
2) the LHCP is synthesized over $k = 1$,

in the broadside direction.

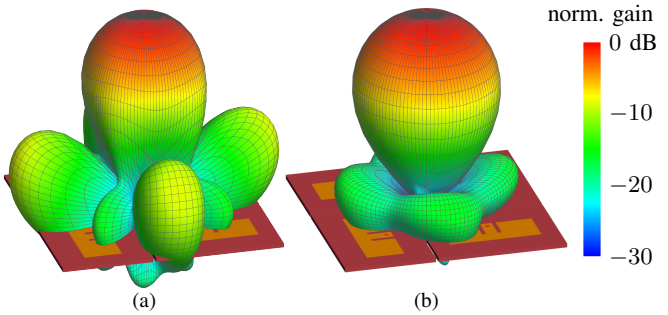

Fig. 4. Simulated radiation patterns: (a) $k = -1$, RHCP, (b) $k = 1$, LHCP.

III. Simulations

An electromagnetic solver was used to simulate the TMAA radiation patterns. Periodically modulated excitations were not supported by the solver, hence the dynamic operation of the switch could not be directly simulated. Instead, the excitations were set as continuous-waves with the amplitudes equal to values of the Fourier-coefficients $G_n^{(k)}$ presented in Fig. 3 and Tab. I. The radiation patterns in the RHCP and the LHCP simulated at the center frequency of the array elements are presented in Fig. 4. Obtained results confirm that the RHCP beam is formed over $k = -1$, and the LHCP beam is formed over $k = 1$.

The sidelobe levels (SLLs) of the radiation patterns presented in Fig. 4(a) and Fig. 4(b) are different due to the cross-polarization components of the array elements. These components interfere constructively for $k = -1$ increasing the SLL, whereas for $k = 1$ they interfere destructively decreasing the SLL. The cross-polarization components also affect the main beam, which results in slightly different beamwidths.

IV. Measurements

The simplified switching model presented in Fig. 2 is valid only to some extent, because the HMC345LP3 SP4T RF switch demonstrates the return loss and isolation of 10 dB and 35 dB, respectively. The non-ideal operation of the switch causes internal reflections of the received signal. In addition, a shape of the pulses is affected by some non-uniform idle time between switching states. This introduces parasitic phase-shifts to the sidebands, which increase with the switching rate. Therefore, the measurements were conducted with a relativity low switching rate of 1 kHz. The fabricated TMAA was measured inside an anechoic chamber in the receive mode. The instrumentation used in the measurements include the Rohde & Schwarz SMF100A signal generator and Keysight N9322C spectrum analyzer.

The radiation patterns were measured with two truncated corner square patch antennas with orthogonal senses of polarization (RHCP and LHCP). Fig. 5 shows radiation patterns measured over $k = \{-2, -1, 0, 1, 2\}$ for the incident wave frequency of 5.32 GHz. Obtained results confirm that the RHCP and the LHCP are realized over $k = -1$ and $k = 1$, respectively. Other sidebands demonstrate significantly smaller gain, especially in the broadside direction.

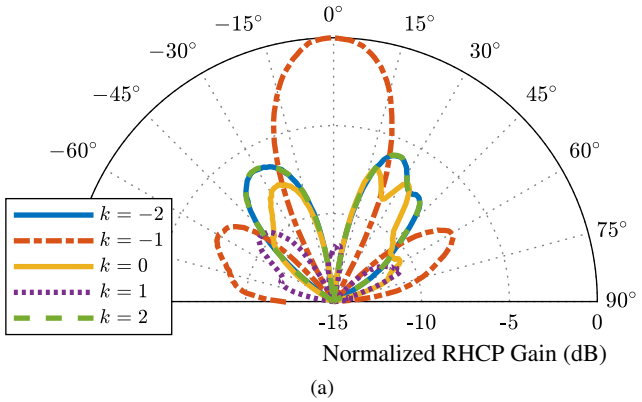

(a)

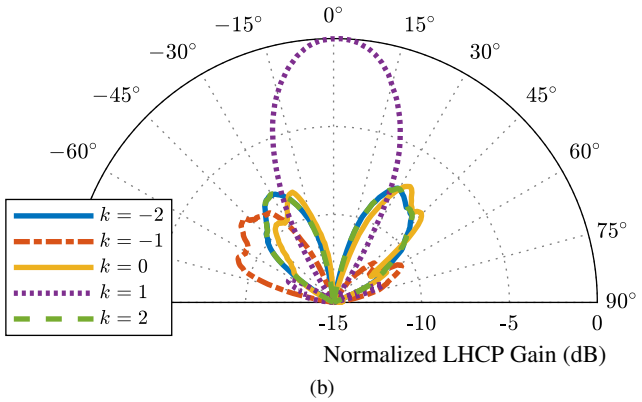

(b)

Fig. 5. Radiation patterns measured in different senses of a circular polarization: (a) RHCP, (b) LHCP; $-90° < \theta < 90°$, $\varphi = 0°$.

The AR was measured according to the polarization-pattern method [2] by rotating a linearly polarized log-periodic antenna in the plane of the polarization and recording the sideband voltage levels. Fig. 6 shows AR measured over $k = \pm 1$ for different frequencies of the incident wave. Obtained values are below 2 dB in the whole frequency band, which reveals that the phase-progression introduced by the time-modulation is independent of the incident wave frequency.

V. Conclusion

The presented TMAA provides orthogonal senses of circular polarization over different frequencies of sideband components. The RHCP and the LHCP are synthesized over the first negative sideband frequency ($k = -1$) and the first positive sideband frequency ($k = 1$), respectively. In addition, the phase-progression introduced by the time-modulation is independent of the RF signal frequency. As a result, the operational frequency range is limited by the performance of elements rather than by the feeding mechanism.

The presented TMAA with a dual-circular polarization is suitable for receiving RF systems and can be used for an automatic conversion of the polarization-diversity into the frequency-diversity. Therefore, the LHCP and RHCP electromagnetic waves can be received and separated, even if they arrive from the same direction and at the same frequency.

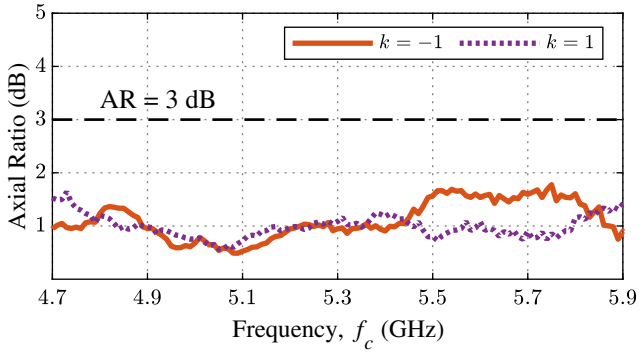

Fig. 6. AR measured in the broadside direction.

References

[1] *Standard for Definitions of Terms for Antennas*, IEEE Std 145-2013 Std., Mar. 2014.

[2] C. A. Balanis, *Antenna theory: analysis and design*. John Wiley & Sons, 2012.

[3] P. S. Hall, J. S. Dahele, and J. R. James, "Design principles of sequentially fed, wide bandwidth, circularly polarised microstrip antennas," *IEE Proc. H - Microw., Antennas Propag.*, vol. 136, no. 5, pp. 381–389, Oct 1989.

[4] J. Huang, "A technique for an array to generate circular polarization with linearly polarized elements," *IEEE Trans. Antennas Propag.*, vol. 34, no. 9, pp. 1113–1124, Sep. 1986.

[5] A. Pal, A. Mehta, and M. E. Marhic, "Generating a pure circularly polarised axial beam from a pattern reconfigurable square loop antenna," *IET Microw. Antennas Propag.*, vol. 7, no. 3, pp. 208–213, Feb. 2013.

[6] Y. Li, Z. Zhang, and Z. Feng, "A sequential-phase feed using a circularly polarized shorted loop structure," *IEEE Trans. Antennas Propag.*, vol. 61, no. 3, pp. 1443–1447, Mar. 2013.

[7] S. X. Ta and I. Park, "Metasurface-based circularly polarized patch array antenna using sequential phase feed," in *Int. Work. Antenna Techn.: Small Antennas, Innovative Structures, and Applications (iWAT)*, Athens, Greece, Mar. 2017, pp. 24–25.

[8] K. Kim, B. C. Jung, and J. Woo, "A compact dual-polarized (CP, LP) with dual-feed microstrip patch array for target detection," *IEEE Antennas Wireless Propag. Lett.*, pp. 1–1, 2019.

[9] I. Słomian, K. Wincza, and S. Gruszczyński, "Series-fed microstrip antenna lattice with switched polarization utilizing Butler matrix," *IEEE Trans. Antennas Propag.*, vol. 62, no. 1, pp. 145–152, Jan. 2014.

[10] P. Rocca, F. Yang, L. Poli, and S. Yang, "Time-modulated array antennas – theory, techniques, and applications," *J. Electromagn. Waves Appl.*, vol. 33, no. 12, pp. 1503–1531, 2019.

[11] R. Maneiro-Catoira, J. Brégains, J. A. García-Naya, and L. Castedo, "Time modulated arrays: from their origin to their utilization in wireless communication systems," *Sensors*, vol. 17, no. 3, p. 590, Mar. 2017.

[12] L. Poli, P. Rocca, G. Oliveri, and A. Massa, "Harmonic beamforming in time-modulated linear arrays," *IEEE Trans. Antennas Propag.*, vol. 59, no. 7, pp. 2538–2545, Jul. 2011.

[13] L. Poli, P. Rocca, L. Manica, and A. Massa, "Time modulated planar arrays - analysis and optimisation of the sideband radiations," *IET Microw. Antennas Propag.*, vol. 4, no. 9, pp. 1165–1171, Sep. 2010.

[14] T. D. Drysdale, B. Allen, and E. Okon, "Sinusoidal time-modulated uniform circular array for generating orbital angular momentum modes," in *11th Eur. Conf. Antennas Propag. (EuCAP)*, Paris, France, Mar. 2017, pp. 973–977.

[15] Y. Q. H. Li, Wen Tao and X. W. Shi, "Synthesis of conformal phased antenna arrays with a novel multiobjective invasive weed optimization algorithm," *Frequenz*, vol. 72, no. 5-6, pp. 209–219, Apr. 2017.

[16] Q. Chen, J. Zhang, W. Wu, and D. Fang, "Enhanced single-sideband time-modulated phased array with lower sideband level and loss," *IEEE Trans. Antennas Propag.*, vol. 68, no. 1, pp. 275–286, 2020.

[17] Q. Zhu, S. Yang, R. Yao, and Z. Nie, "Gain improvement in time-modulated linear arrays using SPDT switches," *IEEE Antennas Wireless Propag. Lett.*, vol. 11, pp. 994–997, 2012.

[18] G. Bogdan, Y. Yashchyshyn, and M. Jarzynka, "Time-modulated antenna array with lossless switching network," *IEEE Antennas Wireless Propag. Lett.*, vol. 15, pp. 1827–1830, 2016.